Interaction of He^+ and Ne^+ ions with Ni(100)-K and Cu(100)-K surfaces having variable potassium coverage

H. D. Hagstrum,* P. Petrie, and E. E. Chaban
AT&T Bell Laboratories, Murray Hill, New Jersey 07974-2070
(Received 16 June 1988)

This paper presents an electron-spectroscopic study employing slow He^+ and Ne^+ ions incident on Ni(100) and Cu(100) surfaces with varying amounts of adsorbed potassium. Investigation of the changes in electron-energy spectra as the work function of the surface is varied probes the pattern of resonance tunneling, excitation conversion, and Auger electron-ejection processes. When the surface is clean the work function ϕ is high and the mode of electron ejection is the two-electron process of Auger neutralization of the incident ions yielding a folded two-electron spectrum. As the macroscopic ϕ is reduced by K adsorption the surface develops more and more regions near K atoms where the local ϕ is small, permitting resonance neutralization of the incident ion to form a metastable atom which on Auger deexcitation ejects electrons in a one-electron spectrum. This paper reports an investigation of this transition from the two-electron, kinetic energy spectrum to the one-electron spectrum and of the specific characteristics of each of these spectral types. Results are compared in detail with a published study by other investigators of the interaction of thermal He metastable atoms with a Cu(110)-K surface having variable K coverage. This comparative study has illuminated the differences observed in the spectra produced by incident 12-eV ions which turn to metastables in the high-K-coverage regime and thermal metastables which turn to ions at low K coverage. We have demonstrated that the local work function of "clean" sites decreases as K coverage increases in the low-coverage regime by interpreting small observed changes in the kinetic energy spectra of ejected electrons. This, in turn, leads to an estimate of the variation of the mean separation of K atoms with increasing K adsorption. We present new data for ion neutralization at the clean Cu(100) surface. From these we obtain the deconvolution of the kinetic energy spectrum that is the initial-state transition density for comparison with photoemission spectra. These results are also compared in detail, particularly with respect to energy broadening, with the results of an investigation by others employing ions descendent from incident thermal metastables.

I. INTRODUCTION

The electronic interactions of ions and metastable atoms with solid surfaces are of interest in their own right since they represent a subfield of particle-solid interactions. Beyond this, however, they underline two of the most surface-specific, electron spectroscopies of solids, namely, those based on ion neutralization (INS), via the process of Auger neutralization (AN), and metastable-atom deexcitation (MDS), via the process of Auger deexcitation (AD). It was not surprising, therefore, to find in earlier work with incident ions that the energetic relationships of filled and empty electronic levels in solids to such levels in the interacting atom were of paramount importance in understanding the properties of INS.[1] The possibility was proposed that an incident ion could be transformed to a metastable atom via resonance tunneling before an electron-ejection process could occur, and this was used to interpret the anomalous variation with ion energy of the kinetic energy distribution and the total yield of electrons ejected from polycrystalline tungsten by Ne^+ ions.

This was, to be sure, not the earliest discussion of resonance tunneling as a precursor state to Auger processes. Massey,[2] and Cobas and Lamb[3] considered the two-stage process of resonance neutralization (RN) of the ion followed by Auger deexcitation (AD) as the mode of electron ejection that would occur for ions incident on high-work-function metals. They arrived at this conclusion because they did not consider the variation of energy levels in the atom caused by image-force interaction. This interaction was first introduced into the discussion of surface, electronic processes by Hagstrum[4] and Varnerin[5] and was later discussed in relation to photoemission[6] as the phenomenon of "relaxation." Precursor resonance tunneling has also been observed in the more recent development of MDS in which the interacting atom is initially metastably excited rather than ionized.[7–13]

In this paper we present the results of a study of the effects of work-function change on the interaction processes for incident ions. The work function has been reduced from the clean-surface value by the adsorption of potassium. Kinetic energy spectra of electrons ejected from Ni(100) and Cu(100) substrates have been obtained for incident He^+ and Ne^+ ions. In addition, spectra for incident He I and Ne I photons are included. As expected, several of the observations with incident ions are corroborative of those made in a study with incident metastable atoms.[14] Interesting differences appear between the spectra for nominally 10-eV ions (12 eV including image-force acceleration) and those for 60-meV metastables. At low potassium coverages, small but definite spec-

tral changes are observed for incident ions that are said not to be observed for incident metastables. These observations lead to estimates of the change of local work function at "clean" sites and of the mean separation of K atoms on the surface. The relative magnitudes of energy broadenings in the ion neutralization spectra for incident ions and for ions descendent from incident metastables have been shown to yield information on the relative distances from the surface at which Auger, and resonance-tunneling processes occur. Novel data demonstrating excitation conversion of He metastables are presented. A preliminary report of some aspects of this work has been given.[15]

The organization of this paper is as follows. In Sec. II we discuss the electron-transition processes and the energy-level variation in the incident atom with surface separation, in terms of which we must interpret our data. Experimental details are given in Sec. III and the data on potassium alkalation of Ni(100) in Sec. IV. The spectral changes for incident ions and photons that accompany K adsorption on Ni(100) are evaluated in Sec. V. This is followed in Sec. VI by a presentation of the work on Cu(100)-K and comparison of it with the work of Woratschek *et al.*[14] employing metastable atoms. Our data on the excitation conversion of He metastables are presented in Sec. VII. Summary and conclusions are in Sec. VIII.

II. ELECTRON TRANSITION PROCESSES

A He^+ ion approaching a solid surface will either be resonance neutralized to an excited state, as a first stage, or Auger neutralized with the ejection of an electron from the filled band of the solid. Which of these occurs depends upon the relative energies of the Fermi level and the lowest-lying excited levels of the He atom. Assuming for the moment a single, excited level, the two possible configurations result in either a one-stage or a two-stage electron-ejection process as is illustrated in Fig. 1. When the work function of the surface is large enough to place the lowest excited He level above the Fermi level only the Auger neutralization process (AN) occurs as in Fig. 1(a). For a low-work-function surface, as in Fig. 1(b), an excited level in the atom will lie below the Fermi level and resonance tunneling into it can occur. This process of resonance neutralization (RN) occurs father from the surface than does any Auger process and thus it becomes the first stage of the two-stage, electron-ejection process. The electron is now ejected from the solid in the process of Auger deexcitation (AD) of the newly formed, excited atom.

The analogous set of one- and two-stage processes that occur for incident metastable atoms is diagrammed in Fig. 2. The direct Auger deexcitation of the metastable can occur for a clean metal surface only if the surface has a sufficiently small work function as in Fig. 2(a). For a high-work-function surface, as in Fig. 2(b), resonance ionization (RI) of the electron from the metastable state is followed by Auger neutralization (AN) of the ion thus produced. This descendent ion approaches the solid more slowly than the incident ions in the present work

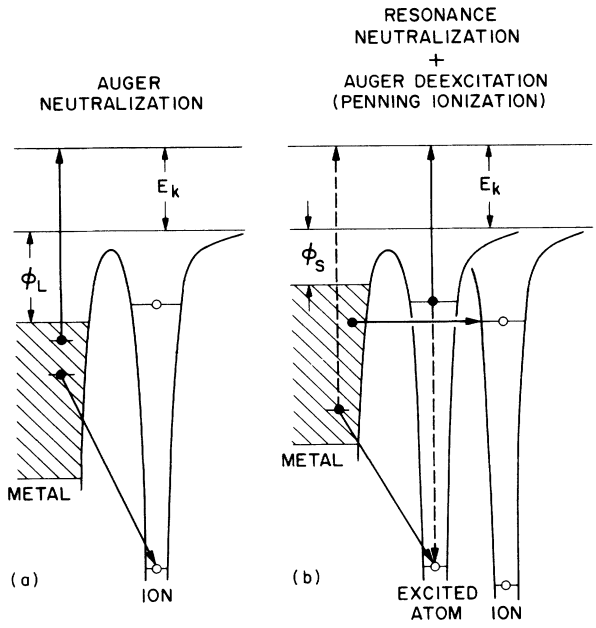

FIG. 1. Electron-energy diagrams for incident ions illustrating at (a) the single-stage process of Auger neutralization (AN) for a high-work-function surface, and at (b) the two-stage process of resonance neutralization followed by Auger deexcitation (RN + AD) for a low-work-function surface.

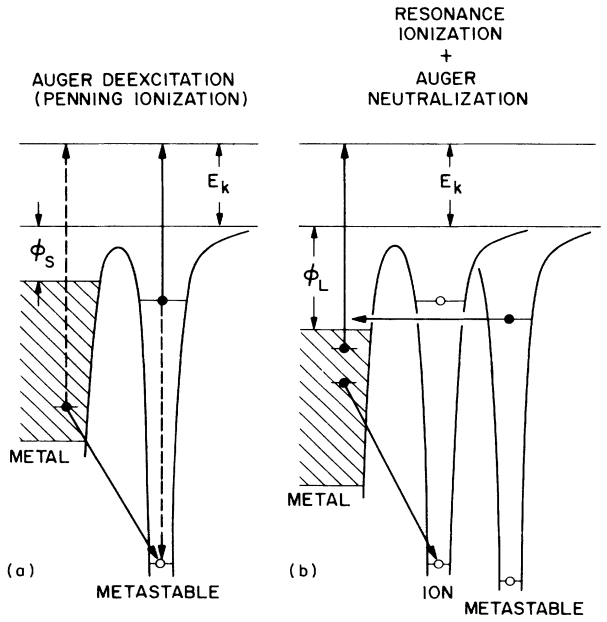

FIG. 2. Electron-energy diagrams for incident metastable atoms illustrating at (a) the single-stage process of Auger deexcitation (AD) for a low-work-function surface, and at (b) the two-stage process of resonance ionization followed by Auger neutralization (RI + AN) for a high-work-function surface.

but are accelerated somewhat by image-force attraction before the AN process occurs. Our data for Cu(100) in Sec. VI afford us the opportunity to discuss the effects of the velocity difference of the incident ions or metastables, since, as indicated above, a study of electron ejection from Cu(110) by thermal metastables has been reported.[14]

The possibility of precursor resonance tunneling leads to confusion in the use of the terms ion neutralization spectroscopy (INS) and metastable deexcitation spectroscopy (MDS) because, although they indicate the nature of the incident particle, these terms do not always specify the process by which electrons are actually ejected from the surface. To avoid this confusion we shall identify processes by the specific designations: RI and RN for resonance ionization and resonance neutralization, AD and AN for Auger deexcitation and Auger neutralization, respectively, and RN + AD and RI + AN for the two possible two-stage processes.

Electron ejection via AD is possible at high-work-function surfaces in some circumstances, however. If above the top of the filled band there is a sufficiently wide energy gap with no allowed electronic states in it, resonance ionization of the metastable electron cannot occur. A second possibility involves the decoupling of the wave function of the metastable level from those of the unfilled levels in the solid by the interposition of a sufficiently "thick" adsorbate having a sufficiently low density of states above the Fermi level of the substrate. We encounter neither of these conditions in the present work, however.

There are two phenomena connected with the atomic interaction with a surface that we shall need in interpreting our results. The first of these is the rise of the atomic energy levels in the atom relative to those in the solid as the atom approaches the surface.[4,5] Since one plots the energy levels relative to the ionization limit this rise comes about because of the image interaction of the final ionic state of each ionization process. Under certain circumstances it makes possible the crossing of the Fermi level by an excited level in the atom at a critical atom-solid separation s_c that lies in the separation range where resonance transitions are possible. In this case resonance neutralization occurs for $s > s_c$, resonance ionization for $s < s_c$.

The second of these phenomena is that of excitation conversion from one excited state to another as the atom approaches the surface.[16–18] The specific case observed is the conversion of excitation from the ^1S He metastable level to the ^3S as the atom approaches a surface. The difference of 0.8 eV in excitation energy is in this case large enough so that the subsequent metastable deexcitation spectra can be resolved. This would not be the case for the two Ne metastables whose excitation energies differ by less than 0.1 eV.

Two types of excitation conversion have been proposed. The first is that in which the two excited states straddle the Fermi level at an atom-solid separation where resonance tunneling is highly probable. This "resonance excitation conversion" (REC) is illustrated in Fig. 3(a) and is the process assumed by Lee *et al.*[17] in their

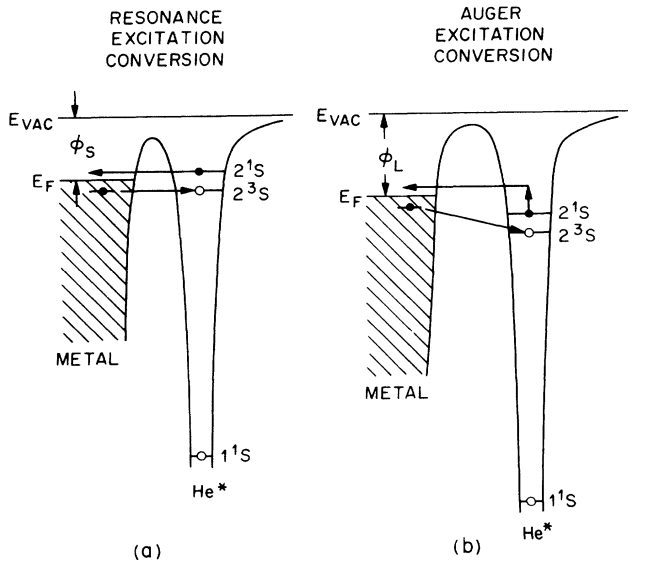

FIG. 3. Electron-energy diagrams illustrating two forms of excitation conversion of He*($2\,^1S$) to He*($2\,^3S$). At (a) is shown resonance excitation conversion (REC) which can occur when the two levels straddle the Fermi level. At (b) is shown Auger excitation conversion (AEC) where the two levels need not straddle the Fermi level. Part (b) of this figure is after Woratschek *et al.* (Ref. 18).

discussion of excitation conversion. The distance range in which the ^1S and ^3S levels straddle the Fermi level, and in which this type of conversion can take place, is the interval between $s_c(^1S)$ and $s_c(^3S)$. This interval can be far from the surface at high work function ϕ but moves close to the surface at low ϕ.

The second type of excitation conversion is that recently proposed by Woratschek *et al.*[18] The electronic transitions of this interesting and important idea are illustrated in Fig. 3(b). This is an Auger-type process in which an electron from the filled band of the solid, on tunneling into the lower ^3S level, loses at least the amount of energy necessary to raise the ^1S electron to a level above the Fermi level where it can tunnel into the solid. The important feature of this "Auger excitation conversion" (AEC) is that it is not restricted, as is REC, to a narrow range Δs of atom-solid separation that moves along the s scale as ϕ is varied. AEC can occur from the largest s at which the respective wave functions overlap sufficiently to give the process some measurable probability to the surface-atom separation $s_c(^3S)$ at which the ^3S level rises above the Fermi level. Woratschek *et al.*[18] point out that for low ϕ surfaces AEC and not REC must occur since the s range for REC lies in, or even closer to the surface than, the range in which the AD process occurs.

The various processes we have been discussing are illustrated in the electron-energy diagram of Fig. 4. Here we plotted the energies of the ground and two metastable states of the He atom relative to their ionization limit, the vacuum level at $E = 0$, as functions of distance of the atom from the image plane outside a metal surface. A low work function ($\phi = 1.5$ eV) is assumed and the elec-

tronic transitions of the four processes RN, AEC, AD, and REC are shown. Also indicted are the critical distances, $s_c(^1S)$ and $s_c(^3S)$, where the effective metastable energy levels at $-E_i'(2\,^1S)$ and $-E_i'(2\,^3S)$ cross the Fermi level at $E=-\phi$.

The energy-level variation we have assumed for each of the three atomic states in Fig. 4 is

$$E_i'(s)(\text{eV})=E_i(s)(\text{eV})-3.6\ (\text{eV Å})/s[\text{Å}]\ . \qquad (1)$$

Here $E_i'(s)$ is the effective ionization energy of the incident ground state or excited atom at a separation s from the image plane of the surface, $E_i(\infty)$ is its ionization energy at infinity, and $3.6/s$ is the image potential at s. The image potential $3.6/s$ is the same as that derived by Appelbaum and Hamann[19] and Lang and Kohn,[20] usually expressed as $3.6/(R-R')$, where $R-R'$, the distance between the ion and the image plane, is expressed in terms of the distance from the ion to the jellium edge, R, and the distance from the image plane to the jellium edge, R'. In writing Eq. (1) we have neglected van der Waals interactions, repulsive interactions in the initial and final states near the surface,[1,12] and electron-electron repulsion.[12] It is agreed, however, that the image potential is the dominant term in the region where electron transitions occur so Eq. (1) is adequate for our pedagogical purposes here.

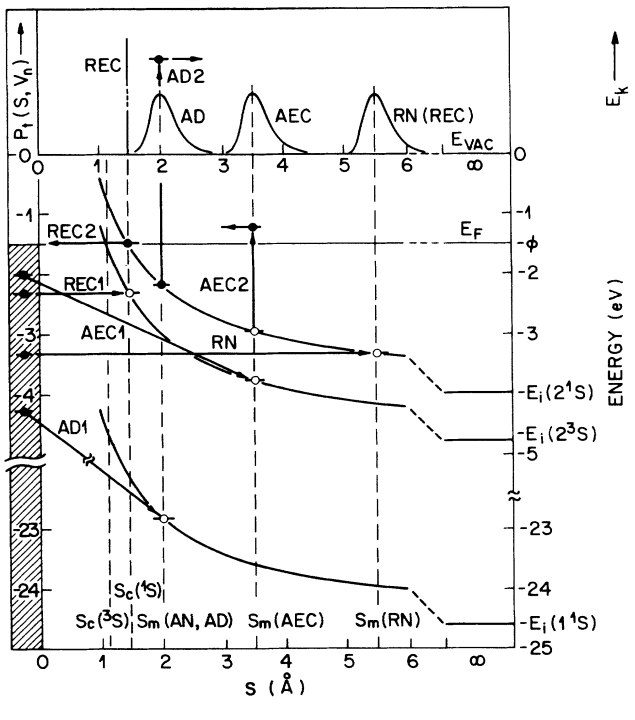

FIG. 4. Electron-energy diagram illustrating the electronic transitions of a number of sequential electronic processes that can occur as an incident ion approaches a surface. The variation near the surface of the three energy levels of the He atom involved in these processes are shown. The $P_t(s,v_n)$ functions plotted above the vacuum level ($E=0$) are discussed in the text. The electronic transitions of the various processes are shown as arrows labeled with the initials of the corresponding process: RN for the one-electron process and AEC1,2; AD1,2; and REC1,2 for the two-electron processes. Also shown are the distances s_m for the RN, AEC, and AD processes and the critical distances s_c at which the ^1S and ^3S He* levels cross the Fermi level at $E=-\phi=-1.5$ eV.

When an AN process occurs at $s=s_m$ the maximum electron energy in the AN electron spectrum is equal to $E_i'(s_m)-2\phi$, where $E_i'(s_m)$ is the effective ionization energy of the ground state at $s=s_m$. Knowing ϕ and having an expression for $E_i'(s)$, Eq. (1) for example, one can obtain a value for the position, s_m, of the ion when the AN process occurs.[1] Sesselmann *et al.*,[12] who obtain E_i' using a method that measures the maximum kinetic energy of both photoemitted and ion-ejected electrons, determined values for R, the separation from the jellium edge. These procedures are of interest here because they bear on the question of the appropriate image-potential formula. Sesselmann *et al.* compare their R for slow He^+ ions descendent from thermal metastable He* atoms incident on Cu(110) with the s_m obtained for 40-eV He^+ on polycrystalline W by Hagstrum.[21] In their discussion of this comparison they confuse s with R by considering Hagstrum's s as an R value and by defining the classical image potential as $e^2/4(R-R')$ with $R'=0$. Appelbaum and Hamann[19] and Lang and Kohn[20] identify s in the expression $e^2/4s\,(3.6/s)$ as $R-R'$, the distance from the image plane, not as R, the distance to the jellium edge. Thus in using the form $3.6/s$ one does determine distances from the image plane even though in early work one did not appreciate this fact.

We also note here that a better choice of early data for comparison with the Cu(110) data of Sesselmann *et al.* is that in Fig. 2 of Ref. 22 for 5-eV ions also incident on Cu(110). There, kinetic energy distributions of electrons ejected by 5-eV He^+, Ne^+, and Ar^+ ions are plotted and linear extrapolations of the high-energy ends to obtain estimates of $E_i'(s_m)$ are indicated. For these ions, respectively, values for $\Delta E_t=E_i(\infty)-E_i'(s_m)$ of 1.9, 1.7, and 1.4 eV were obtained. These are to be compared with the values 2.1, 1.8, and 1.4 eV given by Sesselmann *et al.* in their Table V of Ref. 12 for these ions descendent from thermal metastables. Note that, as should be the case, the ΔE_t values for the faster of the 5-eV ions lie below the corresponding values for the thermal ions by greater amounts.

At the top of Fig. 4 are plotted the $P_t(s,v_n)$ functions for the four electron-transition processes we are considering. Each function, when multiplied by ds, gives the probability that the process occurs in ds at s on the assumption of an exponential transition rate and appropriate parameters.[1] Since the RN, AEC, and AD processes are not restricted to specific ranges of s, these functions have the form given by Eqs. (39) or (44) of Ref. 1. Each peaks at $s_m=(1/a)\ln(A/av_n)$, Eq. (40) of Ref. 1. The s_m values assumed yield reasonable relative placements of the several transition processes based on experimental conclusions concerning the ordering of the processes and the value of the effective neutralization energy of He^+ where the AN process occurs.[12,23] The widths at half maximum of the P_t functions is $2.48/a$ with a equal to 5 $Å^{-1}$. The magnitude of a could well be smaller, 3 $Å^{-1}$, for example, making the P_t function wider. The REC

process, being restricted to a region at $s \leq s_c(^1S)$ where its transition rate is very high, occurs very rapidly in a very narrow range of s. For an exponential rate function, $R_t(s) = A \exp(-as)$, this "s-restricted" P_t function is

$$P_t(s,v_n) = (A/v_n)\exp\{(A/v_n)[\exp(-as_c) - \exp(-as)] - as\} \quad (2)$$

$$= a \exp\{\exp[-a(s_c - s_m)] - \exp[-a(s - s_m)] - a(s - s_m)\} . \quad (3)$$

The corresponding $P_0(s,v_n)$ function, the probability that the particle retains its initial identity, is

$$P_0(s,v_n) = \exp\{(A/av_n)[\exp(-as_c) - \exp(-as)]\} \quad (4)$$

$$= \exp\{\exp[-a(s_c - s_m)] - \exp[-a(s - s_m)]\} . \quad (5)$$

The probability $P_t(s)$ at $s = s_c(^1S)$ for the REC process calculated from Eq. (3) has the very large value of 4×10^7 Å^{-1}. In this calculation the s_m used in Eq. (3) is that the unrestricted P_t for REC taken to be the same as that for RN whose maximum value at its s_m is $0.368a$ [Å^{-1}] $= 1.84$ Å^{-1}. Equations (2)–(5) are restricted to $s \leq s_c$.

III. EXPERIMENTAL DETAILS

The experimental apparatus used in this work is depicted schematically in Fig. 5. It is a modification of earlier apparatus[23] necessitated by the installation of the source of K^+ ions. The apparatus provides for the electron spectroscopies based on ion neutralization at port 1, ultraviolet photoemission at port 4, and core-level Auger electron spectroscopy using the electron gun placed 15° off the port 4 axis. It also includes low-energy electron diffraction at port 3, sputtering gear at port 2, as well as evaporators and gas-inlet arrangements at ports 2 and 3.

The new addition to the apparatus is the K^+ ion source placed between ports 1 and 2. The source is an indirectly heated potassium aluminosilicate molecular sieve of the type described by Weber and Cordes.[24] That used in this work was purchased from Spectra-Mat Inc., Watsonville, California, described by Heinz and Reaves.[25] Dr. Weber kindly provided us with the design of a gun used with their alkali sources but not described Ref. 24. It is of the form shown in Fig. 5. The porus tungsten plug, which we shall term electrode S and show cross hatched in our figure, is impregnated with the K^+ emitter material. When indirectly heated the source emits K^+ ions that are drawn out by a potential on a first grid, G_1, focused by a three electrode lens system, E_1, E_2, E_3, and passed through a second grid G_2 to the tar-

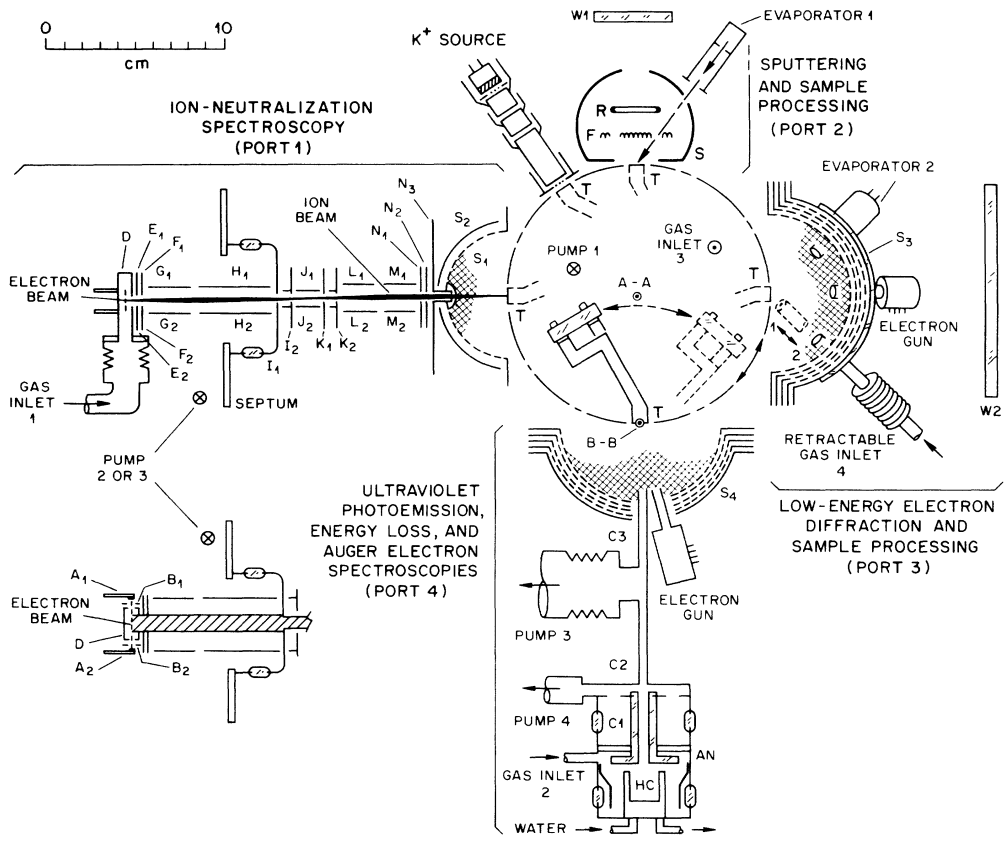

FIG. 5. Schematic diagram of the experimental apparatus. This is a top view except for the apparatus attached to ports 1 and 3, where side views are shown for greater clarity.

get T. The grids are made of 0.025-mm wire spaced 0.25 mm apart. G_1 has a circular aperture 8 mm in diameter, G_2 a 6-mm square aperture oriented with sides parallel to those of the target. The three lens electrodes are made of 12-mm tubing of lengths 10, 10, and 27 mm, respectively. All electrodes are mounted on three 3-mm diameter Al_2O_3 rods.

This type of alkali source produces ions making possible relative measurement of surface dosage. Since our target is connected to a sensitive current meter we can integrate the target current to obtain the K^+ ion dose. The source lens system is operated at two sets of electrode potentials, one corresponding to "gate closed" with no K^+ incident on the target, and the other to "gate open" when the target is dosed. To specify the electrode potentials we define a format and give the voltages as follows: electrode(s): gate open voltage (gate-closed voltage),

$$S{:}+36(+36)\ ;\quad G_1,G_2{:}0(+66)\ ;$$

$$E_1,E_3{:}-10(-10)\ ;\quad E_2{:}-130(-130)\ .$$

Our exposure rate was such that we could produce the Ni(100)-K surface of minimum work function in about 7 min with an exposure of about 4×10^{-5} A s of K^+ ions. Andersson and Jostell[26] have determined that this occurs at a coverage Θ of 0.2, assuming Θ to be unity at the atom density of the Ni(100) substrate. Since one A s of K^+ corresponds to about 6×10^{19} ions delivered through an aperture of about 40 mm^2, we derive $\Delta\Theta=0.1$ per 10^{-5} A s of K^+ assuming that all of the atoms stay in the area of which they land. The 4×10^{-5} A s dose then gives $\Theta=0.4$ instead of Andersson and Jostell's 0.2 indicating that the K^+ ions spread over a larger area than where they land.

The temperature indicated by a thermocouple on the source heater body is in the range 820 to 850 °C for an exposure at the above rate. Outgassing of the source was carried out at temperatures as high at 940 °C for periods as long as overnight. The manufacturer states that the source can be heated to 1200 °C without damage. Our outgassing was done with the electrode potentials in the gate-closed configuration which apparently resulted in no appreciable ion loss. The Spectra-Mat people state that the only impurity in their K^+ source is Na^+ which after a few hours running drops to a proportionality low value. Weber and Cordes[24] quote Na^+ impurities in their K^+ source as low as four parts per 10^4. It is clear, however, that high-temperature processing of this type of source is essential. When this was done the source performed very well indeed and we have found no spurious peaks in our electron spectra attributable to adsorbed impurities from our K source.

In the sputtering gear at port 2 ions drawn to the target for sputtering are formed in Ne gas by the impact of electrons emitted from the filaments F and accelerated to the ring R.

Our background pressure in the low 10^{-10} or high 10^{-11} Torr range makes possible the low decay rate of the AN electron spectrum from clean Ni(100) shown in Fig. 6. Note in the figure caption the relatively long times required to alter the spectral shape or work func-

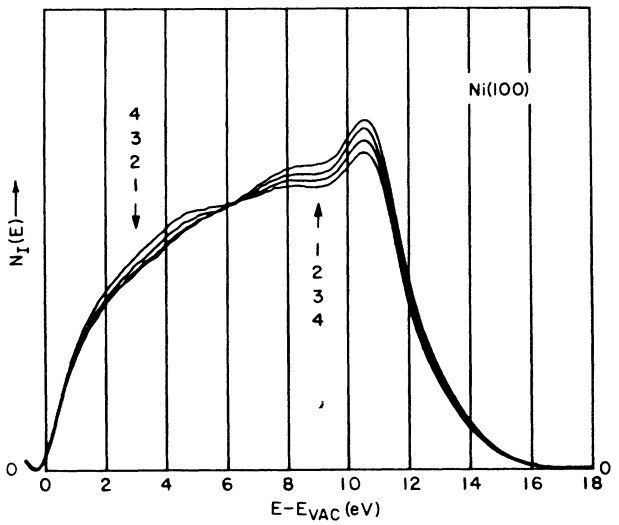

FIG. 6. Kinetic energy distributions of electrons ejected from clean Ni(100) in the Auger neutralization of 10-eV He^+ ions as this surface is degraded by the adsorption from the background gas in the apparatus. Times at which each 40-s run was started after the completion of a target flash to 900 °C are curve 1, 1.2 m; 2, 15 m; 3, 30 m; 4, 50 m. Accompanying work-function change was curves 1–2, 0.072 eV; 1–3, 0.097 eV; 1–4, 0.128 eV.

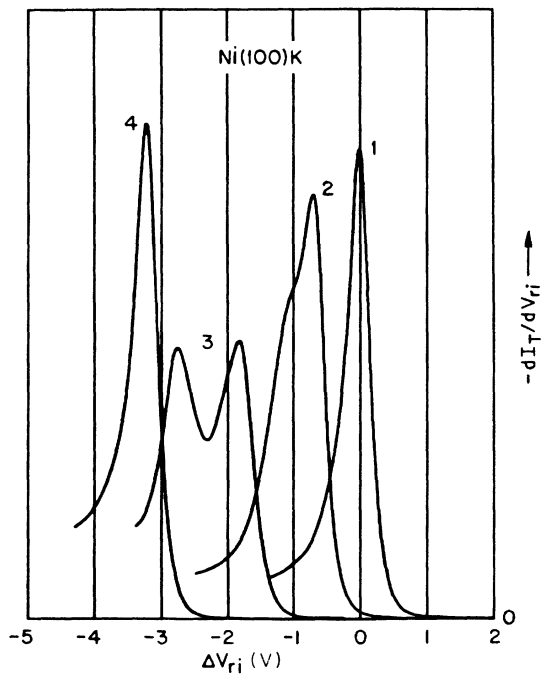

FIG. 7. Plots of the derivatives of He^+ ion-current-retardation curves, $-dI_T/dV_{ri}$ vs ΔV_{ri}, for a series of potassium coverages on Ni(100) at room temperature. The shifts in the maxima of these curves indicate the reductions of surface work function as more K^+ is adsorbed in exposures that for curves 1, 2, 3, and 4 are 0, 1, 3, and 8×10^{-5} A s, respectively. Note the double-peak character of the intermediate curves indicating two patches of differing work function.

tion appreciably. The experimental curves of Fig. 6, like all those of other figures in this paper, are photographic reproductions of analog x-y recorder plots of single runs. Each run is taken at the rate of 2 s per eV of the abscissa scale.

Finally, we cite our three methods of measuring work-function change. The first method involves the retardation of our well-focused ion beam at the target surface. We plot the derivative of the ion current to the target as a function of the retarding voltage that is ramped through the region in which the beam is reflected. As can be seen in Fig. 7, this function for a surface of uniform work function has a sharp peak whose position can be read on the large recording graph paper to one or two hundredths of an electron volt. The change in retarding potential ΔV_{ri} from its value for curve 1 for the clean surface is equal to the change in work function. The second method determines the variation relative to the Fermi level of the vacuum level cut-off point of an electron kinetic energy distribution. The third method determines $\Delta\phi$ from the change in width, ΔW, of a photoemission energy distribution: $\Delta\phi=\hbar\omega-\Delta W$. Our first method has the distinct advantage of being able to detect patchiness of surface work function. The other two methods determine only the lower work function if patchiness exists but are useful as corroborators. Our method of locating an extremum of an electron energy spectrum is to extrapolate linearly to the minimum level of the function the slope of the rather long, straight-line portion of the function at the point of inflection closest to the extremum.

IV. POTASSIUM ALKALATION OF Ni(100)

Potassium was adsorbed on the Ni(100) surface using two different procedures. If the first of these, K^+ ions were adsorbed in discrete amounts after the target had been flashed to 900 °C and cooled nearly to room temperature. We found little difference between accumulative adsorption, in which increments of adsorption were added to each other without intermediate flashing, and successive adsorption, in which each differing quantity of K was administered independently following a target flash to 900 °C. What we did find of importance, however, was the temperature during adsorption since each of these procedures resulted in a surface patchy with respect to work function.

In Fig. 7, as indicated above, we plot the derivative of ion current to the target with respect to retarding voltage as the beam passes through zero velocity at the target surface. The abscissa scale is $\Delta V_{ri}=V_{ri}-V_{ri}(\text{clean})=\Delta\phi$. Curve 1 for the clean surface is obtained after a flash to 900 °C. Curves 2, 3, and 4 correspond to increasing incremental coverages of K of 1, 3, and 8×10^{-5} A s, respectively. Note that the two intermediate coverages show double peaked, retardation derivatives, thus clearly indicating two types of surface patch of appreciably different work function. Note also that at the highest coverage the patches have coalesced into a surface of uniform work function.

The shifts in the peak positions of the retardation derivatives of Fig. 7 can be used to plot work function versus K^+ exposure since the clean surface ϕ is 5.22 eV. Such a plot for the data of Fig. 7 and other intermediate data is shown in Fig. 8. The ion-retardation data are plotted as solid circles and fall on two curves that diverge from one another at small exposure and do not come together until the exposure has reached 6×10^{-5} A s. Plotted as open circles in Fig. 8 are values of ϕ obtained by our second method. These points agree very well with the lower ϕ points from the ion-retardation method.

The results just presented indicated clearly that we should adopt an adsorption procedure that would increase the mobility of K^+ on the surface if we were to form a surface of uniform, macroscopic work function. This could be done either by holding the surface at a temperature sufficiently above room temperature during exposure, or by making the initial exposure the maximum one, and then following it with sequential removal of potassium by thermal desorption. We decided to use the latter procedure. Data illustrating this method are shown in Fig. 9. Here V_{ri} is plotted against the target temperatures used to produce systematic reduction of the K coverage. The open circle at $V_{ri}=10.27$ V, $T=900$ °C is for the clean surface after a flash to 900 °C before K^+

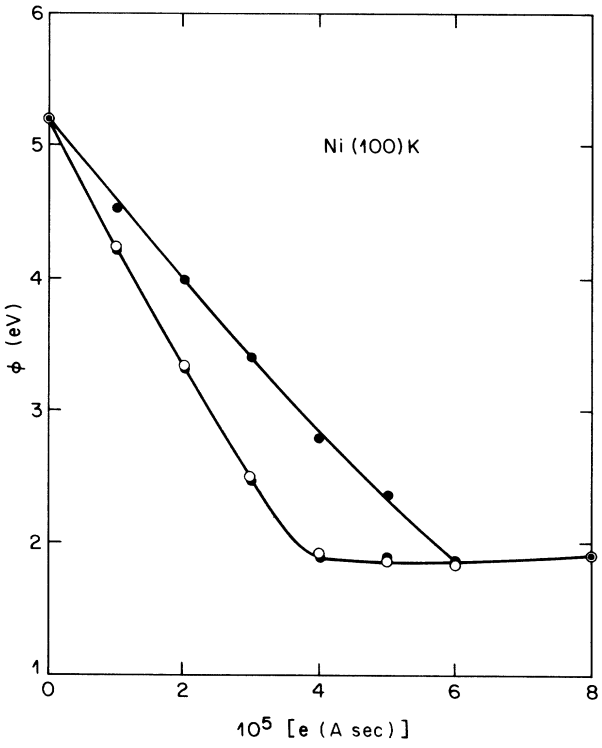

FIG. 8. A plot of work function of Ni(100) vs K^+ exposure at room temperature obtained from measurement of work-function change assuming the clean surface ϕ to be 5.22 eV. Data from the shift in the maxima of the ion-retardation derivatives (Fig. 7) are plotted as solid circles and indicate a surface having two patches of differing work function until the exposure has reached 6×10^{-5} A s. The open-circle data were obtained from the shifts of the vacuum-level cutoff of the kinetic energy distributions of electrons from the AN ejection by He^+ such as those in Fig. 11. Note that this is a plot of ϕ vs K exposure, e, not K coverage, Θ.

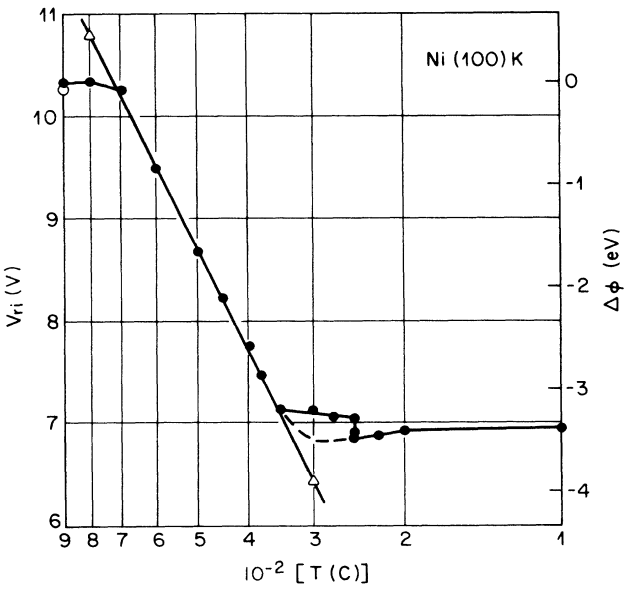

FIG. 9. Plot of V_{ri}, the voltage at the maximum of the ion-retardation derivative curve, as a function of the temperature of successive target flashes used to reduce systematically the coverage of K atoms on Ni(100) after an initial exposure of 10^{-4} A s as explained in the text.

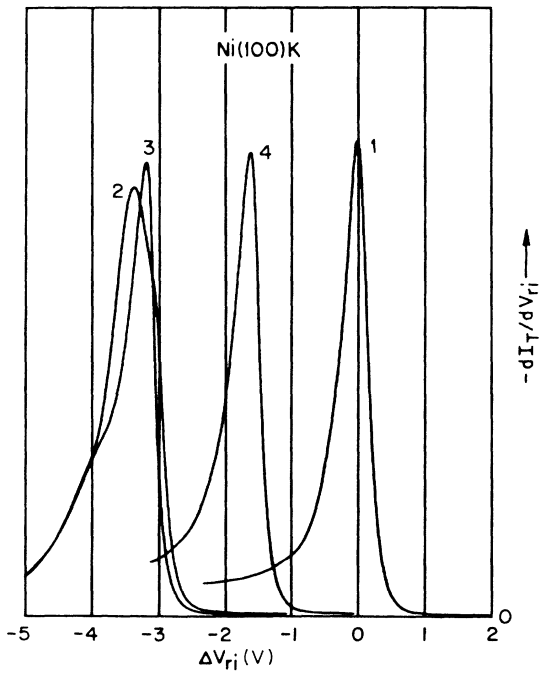

FIG. 10. Plots of the ion-retardation derivative functions the positions of whose maxima are plotted in Fig. 9. Note that the sharp, single-peaked character of these plots indicates uniform, nonpatchy K^+ coverage of the surface. Note also that we cannot plot ϕ derived from these data as a function of either exposure or coverage.

exposure. The point at $V_{ri}=6.95$ V, $T=100$ °C is that obtained after a K^+ exposure of 10^{-4} A s and a single flash to 100 °C. A single flash was made at each temperature where points are shown except for $T=250$ °C where nine flashes occurred, three of which are plotted. The clean surface was recovered by the flashes to $T=700$ °C and above. It is remarkable that between 350 and 700 °C the data lie of the line: $V_{ri}=\phi+10.33=4.44\ln(T)-18.89$.

The retardation derivatives obtained when the sequential removal method of K coverage is used are shown in Fig. 10. Curve 1 is that obtained after target flashes to 900 °C either before K adsorption or after sequential desorption ending with a flash again to 900 °C. Curve 2 is that for maximum exposure. It corresponds to the point at $T=100$ °C of Fig. 9, and curve 3 to that at 350 °C at the start of the logarithmic straight line. Curve 4 is that for the 500 °C point and is representative of such a plot for all points on the logarithmic straight line. We cannot plot ϕ versus coverage Θ from our own data but we can obtain Θ corresponding to our ϕ from the work of others as we do in Secs. V and VI.

V. ELECTRON EMISSION SPECTRA FOR INCIDENT IONS ON CLEAN AND ALKALATED Ni(100)

The changes that take place in the kinetic energy distribution of electrons ejected from Ni(100) when its surface is exposed to increasing amounts of potassium are shown in Fig. 11. Curve 1 is for the clean surface and the increasing ordinal numbers of the curves above it indicate increasing amounts of adsorbed K. The spectra of Fig. 11, however, were obtained during the sequential desorption procedure of Figs. 9 and 10. Thus, when the clean surface was exposed to 10^{-4} A s of K^+, the electron spectrum changed from curve 1 to curve 8 which was then recorded without any heating. Curves 7 through 1 were obtained by successive heatings to increasing temperatures as was done to obtain the data of Fig. 9. Note how the low-energy cut-off points of the kinetic energy distributions shift toward the Fermi level at $E-E_F=0$ as K coverage increases (curve ordinal number increases) and work function decreases.

Curve 1 of Fig. 11 for the clean surface is a two-electron spectrum from the AN process of Fig. 1(a). The deconvolution of earlier data of this type,[27] and of curve 1 of Fig. 16 in Sec. VI of this paper, produce the initial-state, transition-density function whose principal component is the convolution mean of the local densities of states at the surface and at the ion.[22] At the coverage of curve 5 there is sufficient adsorbed K to reduce the work function to the point where the two-stage RN + AD process of Fig. 1(b) can occur yielding a one-electron spectrum. The principal feature of the spectra of curves 5–8 is the peak at the high-energy end of the distribution that is made up of electrons ejected from the relatively small, filled portion of the K 4*s* resonance level that lies below the Fermi level. These are the same basic features observed by Woratschek *et al.*[14] for metastable atoms incident on Cu(110) as K is adsorbed, in which case the sequence of processes is RI + AN at low-K coverage and

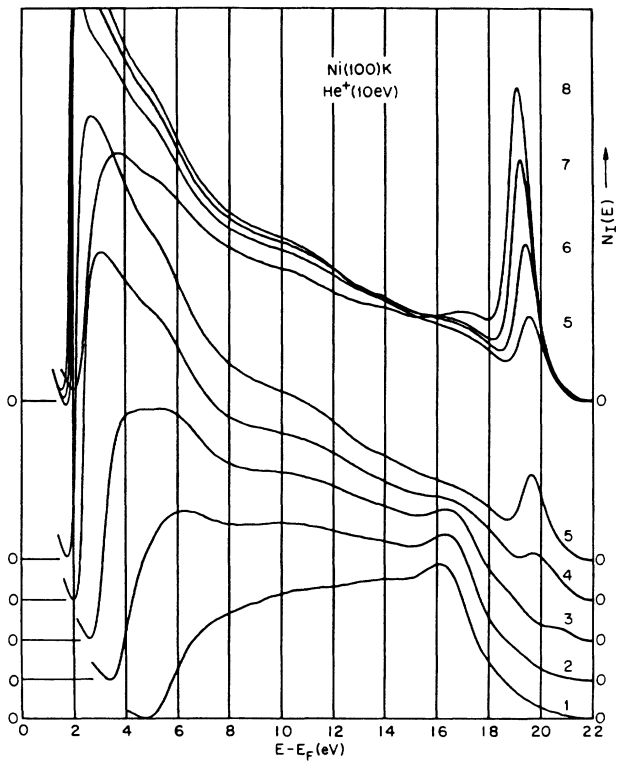

FIG. 11. Kinetic energy distributions of electrons ejected from Ni(100) by Auger neutralization of the incident He^+ ions or by Auger deexcitation of the descendent He^* metastable atoms formed from the incident ions by resonance neutralization (RN). Curve 1 is for the clean surface and curves 2–8 for surfaces with increasing amounts of adsorbed K. Note that curve 8 is obtained after an exposure to 10^{-4} A s of K^+ ions and curves 7–1 after successive amounts of K^+ thermal desorption as described in the text.

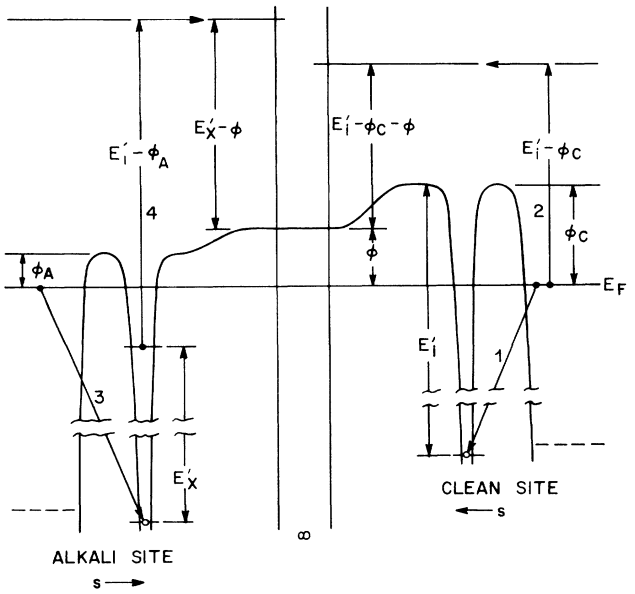

FIG. 12. Electron-energy diagram indicating the energetic relationship of two sites on a partially K covered metal surface. At the left is a site just outside an adsorbed alkali atom (not shown) where the local work function, ϕ_A, is small. At the right is a clean site where the local work function, ϕ_c, equals that of the clean surface. Note the arrows that indicate the direction of increase of distance s from the surface toward infinity at the center of the diagram.

AD when ϕ has been reduced sufficiently at higher-K coverage.

The spectra of curves 1–5 in Fig. 11 document the transition from AN to AD electron ejection and reveal a number of interesting facts. This is the region of low-K coverage in which there are two distinct types of atomic sites on the surface differing appreciably in local work function as is shown in the electron-energy diagram of Fig. 12. That this type of local modification of the surface work function occurs on potassium adsorption has been demonstrated by Lee *et al.*[28] and Woratschek *et al.*[14] using incident metastable atoms.

In discussing the features of a progression of measured electron kinetic energy spectra in terms of the electronic structures of two different surface atomic sites it is essential that one plot the spectra on the energy scale whose zero is at the Fermi level, E_F, the only energy level common to both sites. This is done in Fig. 11 and other such plots. In this way one basically eliminates the macroscopic work function ϕ which depends on the relative areas of alkali and clean sites and is therefore an extrinsic variable with respect to the local-energy structure of alkali and clean sites, at least at sufficiently low alkali coverage. Note that $E-E_F=E_k+\phi$, where E_k is the electron kinetic energy well outside the surface whose macroscopic work function is ϕ.

When K coverage is small, an ion incident upon a clean site remains an ion until it undergoes AN, and the electrons then ejected have essentially the same energy distribution above the Fermi level as they have when the surface is clean. Thus, at a clean site the local work function, the energy by which the flat region of the potential immediately adjacent to a Ni atom lies above the Fermi level, is close to the macroscopic work function of a completely clean surface. The local character of the AN process is evidenced by the fact that the peak at $E-E_F=16.2$ eV in curve 1 of Fig. 11, a feature of the electron kinetic energy spectrum for the clean surface resulting from the AN process, largely retains its form and energy position in spectra for which the density of adsorbed K has increased sufficiently to decrease the macroscopic work function by 2.55 eV. This is the same phenomenon observed and discussed by Woratschek *et al.*[14] for metastable atoms incident on Cu(110).

Woratschek *et al.*[14] state that the AN feature in their spectra for Cu(110) does not shift as ϕ decreases on initial K adsorption. In our curves 1–4 of Fig. 11 for Ni(100), however, we see that as the density of adsorbed K increases, the peak of the AN feature does shift by small but measurable amounts from $E-E_F=16.2$ eV, its position in curve 1. This must arise because the local work function at intermediate sites, even those farthest from adsorbed K atoms, cannot remain exactly at the clean surface value as the surface density of K atoms increases. How this comes about is illustrated in Fig. 13. At (a) in

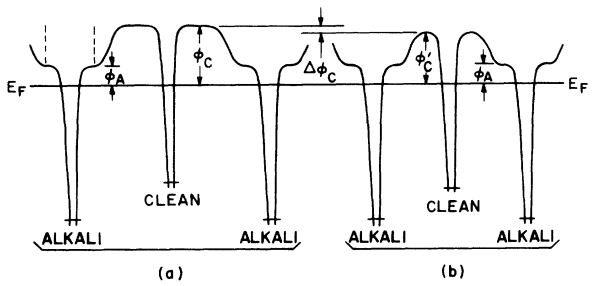

FIG. 13. Two diagrams of the potential variation along a line through two adjacent alkali sites between which there lie clean-surface sites. At (a) the density of alkali sites is small enough such that the clean sites between the alkali sites are the same as those on a completely clean surface. At (b) the density of K atoms is large enough so that clean sites between them are modified somewhat due to proximity to K atoms resulting in a lowered local work function, ϕ'_c.

this figure is shown the situation when the K concentration is relatively small and the distance between adjacent K sites is large enough to allow the local potential over a large area between K sites to be that characteristic of the clean surface. Then the local ϕ_c equals the macroscopic ϕ of the clean surface. The vertical, dashed lines at the left-most alkali site in Fig. 13(a) are meant to suggest that the range over which an adsorbed K atom dominates the surface potential is short.[29] As K concentration is increased and K sites come closer to each other, the local work function at intermediate clean sites decreases to values ϕ'_c below ϕ_c as is shown in Fig. 13(b). Consider the clean-site, right-hand diagram in Fig. 12. Since the vacant ground level of the He atom must lie below the local "vacuum level" by the He ionization energy we see that reduction of the local work function to ϕ'_c increases the transitions 1 and 2 of the Auger process from $E'_i-\phi_c$ to $E'_i-\phi'_c$. It is this that produces the shifts S of the AN spectral feature to energies farther above E_F as is observed in Fig. 11. At higher K concentrations ϕ'_c also varies more with position between adjacent K sites causing the spectral feature to broaden. It is remarkable that both of these effects can be seen in curves 1–4 of Fig. 11. Equating $\phi_c-\phi'_c$ to S yields an average value of ϕ'_c since S for a broadened AN feature is also an average.

Measured energy shifts S[eV] of the peak of the AN feature in the spectra of Fig. 11 and intermediate spectra are listed in Table I. Our procedure for determining these shifts from our kinetic energy spectra was as follows: Two x-y recorder plots of the spectra are placed on a light box with the peaks of the AN features superimposed. The two peaks are considered to be superposed when at their point of contact the tangent lines to the two curves coincide. In this configuration the shift S is the distance d (mm) measured between the vertical line markers on the two plots, each indicating a point 30 eV above the Fermi level. We may write S[eV]$=0.0787d$ (mm) since the size of the energy scale of the original plots is 2

TABLE I. Energy shift S of the AN feature in the spectra of Ni(100)-K (Fig. 11) and the corresponding mean separation R of K atoms.

Curve[a]	$-\Delta\phi$ (eV)	ϕ (eV)	$S=\phi_c-\phi'_c$ (eV)	Θ_K[b]	R[c] (Å)
1	0.00	5.22	0.00	0.000	∞
	0.83	4.39	0.17	0.022	18.1
2	1.64	3.58	0.29	0.048	12.2
	2.10	3.12	0.35	0.068	10.3
3	2.55	2.67	0.38	0.087	9.1
	2.84	2.38	0.40	0.103	8.4
4	3.19	2.03	0.58	0.135	7.3
5	3.33	1.89		0.1	6.7
6	3.41	1.81			
7	3.48	1.74			
min ϕ[d]	3.49	1.73			
(min ϕ)	(3.55)	(1.67)		(0.20)	
	3.48	1.74			
8	3.36	1.86			

[a]A number in this column indicates the spectrum in Fig. 11 to which the data of the line corresponds. The lines without numbers in this column contain data for spectra intermediate to the spectra of Fig. 11.

[b]The relative potassium coverage obtained from the Θ_K versus $\Delta\phi$ plot for the Ni(100)-K of Fig. 2 of Andersson and Jostel, Ref. 26. At $\Theta_K=1$ the density of K atoms would equal that of Ni atoms on the Ni(100) substrate.

[c]The mean separation R of K atoms in hexagonal symmetry for K at low coverages Θ_K is obtained from the relation $\Theta_K=2a^2/\sqrt{3}R^2$ (Ref. 26). Since the edge a of the square surface unit mesh of Ni(100) is 2.49 Å we obtain $R=2.68/\sqrt{\Theta_K}$.

[d]The data on this line are for the point of minimum ϕ in our data. They are very close to the data of Fig. 2, Ref. 26, listed on the next line below, justifying our use of the Andersson and Jostell data to obtain Θ_K from our $\Delta\phi$.

eV per 25.4 mm. The range of the S values in Table I thus involved measurements of lengths between 2.2 to 7.4 mm for which we employed a Gerber variable length scale and optical magnification.

If we can determine the relative coverage Θ_K of K atoms from our values of $\Delta\phi$ we can obtain the mean separation R of K atoms on the surface for each shift S. We have done this using the $\Delta\phi$ versus Θ_K plot of Ni (100)-K in Fig. 2 of Ref. 26. The results are tabulated in Table I. That our data for $\Delta\phi$ are of comparable accuracy to those of Andersson and Jostell[26] is evidenced by the fact that our value at minimum ϕ is very close to theirs. Here we also used a Gerber variable scale and optical magnification in reading Θ_K values from the plot of Andersson and Jostell.

Having Θ_K we can determine R since Θ_K can be expressed in terms of R for ordered, adsorbed K. For the hexagonal or square lattice, respectively, Θ_K equals a^2/R^2 or $2a^2/\sqrt{3}R^2$, from which we obtain in angstroms $R=2.68/\sqrt{\Theta_K}$ or $R=2.49/\sqrt{\Theta_K}$ using $a=2.49$ Å for the unit mesh edge of Ni(100). The distance between centered "clean" sites farthest from K atoms is R or $2R/3$ for the square or hexagonal lattice, respectively. The R values in Table I are for the hexagonal lattice.

We see in Table I that when Θ_K has increased to 0.14, R for the hexagonal lattice has reduced to approximately 7 Å. For this lattice the distance between clean sites farthest from the K atoms is then about 5 Å. For a square lattice at this Θ_K, the distance between K atoms, R, and the distance between clean sites would both be close to 7 Å. At this point, where Θ_K is 0.14, the local ϕ_c' at clean sites is about 0.6 eV smaller than ϕ_c of the clean surface. We believe this result to be reasonable in light of the theoretical finding of Lang *et al.*,[29] whose contour plots in Fig. 2 show that "the electrostatic potential dies out rapidly around 6–7 bohr (<4 Å) from the alkali atoms." The breadth of the AN peak feature in curve 4 of Fig. 11, however, indicates that the local work function varies greatly over that region between K atoms in which AN is still possible. In the spectrum of curve 5 in Fig, 11, at which R has reached 6.7 Å, there is little evidence of an AN feature and a sizable peak of K 4s electrons had appeared indicating that the transition to a one-electron AD spectrum is essentially complete.

At an alkali site, also depicted in Fig. 12, the local work function is at least as small as the smallest macroscopic work function achieved on K adsorption. Thus as K^+ is adsorbed we expect the first RN + AD process to occur for ions that are incident directly above K^+ ion where the local work function is the smallest. At this point the local density of filled electron states just below the Fermi level would be strongly enhanced if a tail of the K 4s electron resonance extended somewhat below E_F.[30] If, in Fig. 4, we move toward the surface along the horizontal line at $E=-\phi$ we see that the ^1S level rises to the level of these K 4s electrons before the ^3S level does. Then RN of He^+ could occur, forming $He^*(^1S)$, some of which might eject electrons via the AD process. Curve 3 of Fig. 11 displays a small, reproducible peak near $E-E_F=20.6$ eV, the energy available from Auger deexcitation of $He^*(^1S)$. This observation supports the idea that an alkali atom adsorbed on a metal at very low coverages is not completely ionized.[30] Since the ^1S level quickly rises above the Fermi level, RI of the newly formed metastable is also possible followed by AN. AEC may yield some $He^*(^3S)$ which, if not immediately resonance ionized, could undergo AD to produce electrons of kinetic energy near 19.8 eV. There is no convincing evidence for this in curve 3, however.

Under the conditions of curves 5–8 of Fig. 11 almost all of the neutralized ions reach the ^3S metastable state before AD occurs. Since the work function for these curves is near its minimum value, excitation conversion must occur via the AEC process. Only when ϕ is in the range 3.3 to 4.2 eV do the ^1S and ^3S energy levels straddle the Fermi level making resonance excitation conversion (REC) possible. Spectra presented in Sec. VII indicate, however, that a tiny portion of metastables do survive as ^1S until AD occurs.

Curves 5–8 are plotted on the same ordinate scale in the upper half of Fig. 11 to show the relation of the K 4s electron peaks to one another as the amount of K on the surface is increased. The peak grows in area and width keeping its high-energy side fixed at the Fermi level. This is exactly what should occur if the peak we observe is the low-energy, filled portion below the Fermi level of a

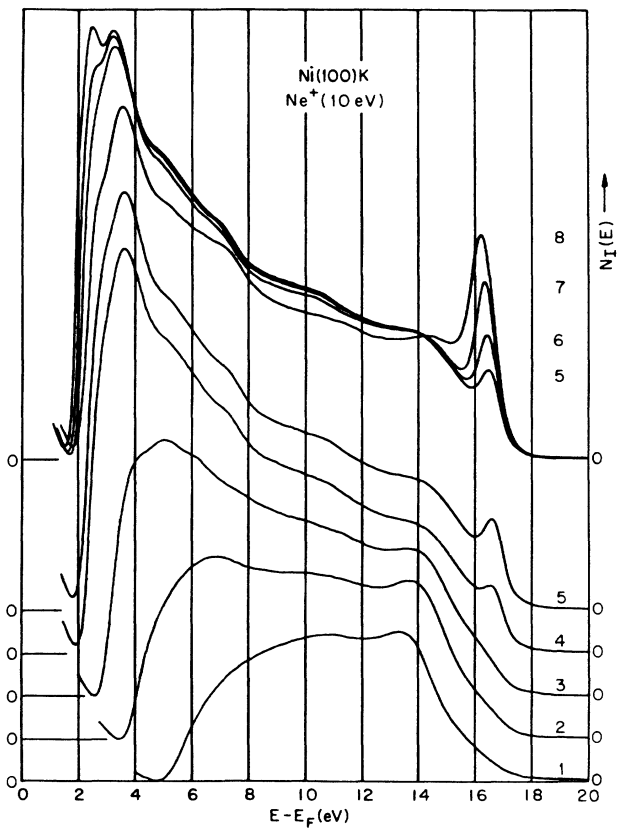

FIG. 14. Kinetic energy distributions of electrons ejected by incident Ne^+ ions, or descendent Ne metastable atoms, from Ni(100) with varying amounts of adsorbed K. This figure is analogous to that of Fig. 11. The K^+ exposure for curve 8 is 10^{-4} A s. K desorption by suitable heatings of the target produced the concentrations yielding curves 7–1.

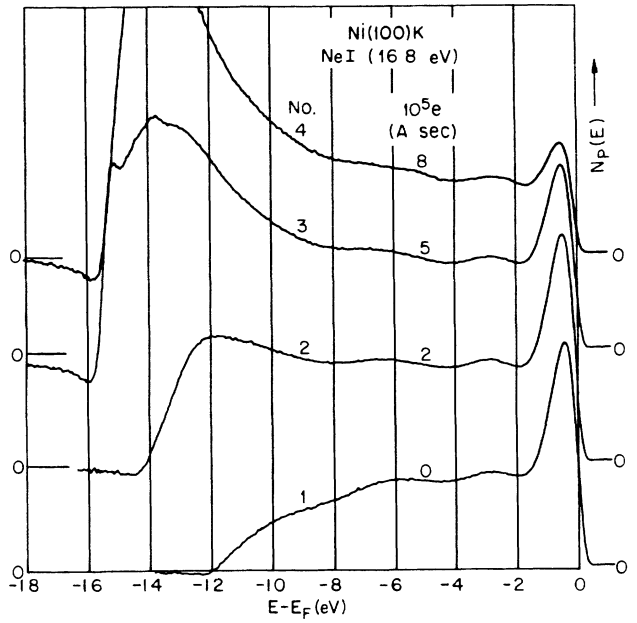

FIG. 15. Kinetic energy spectra of electrons ejected by Ne I photons from Ni(100) with varying amounts of K adsorption. Exposures to produce each curve by adsorption upon the clean surface are given in A s at each curve.

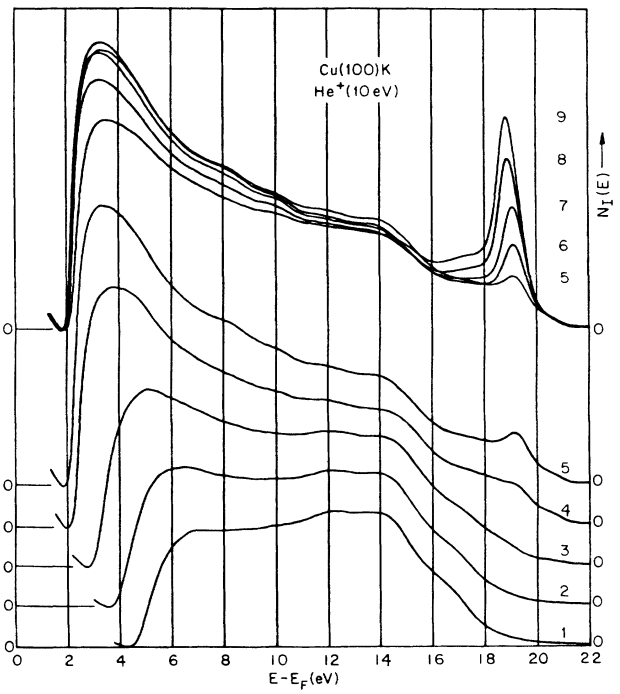

FIG. 16. Kinetic energy distributions of electrons ejected by incident He^+ ions, or descendent He metastable atoms, from Cu(100) with varying amounts of adsorbed K. The K^+ exposure for curve 9 is 8×10^{-5} A s and curves 8–1 were achieved from it by suitable heatings of the target.

much broader resonance, unfilled above the Fermi level, that moves down in energy with increasing K coverage. This is another confirmation of the quantum-mechanical model of Gurney.[30]

Figure 14 presents a series of spectra for incident Ne^+ ions as K^+ is administered to the Ni(100) surface. It demonstrates again all the phenomena discussed for incident He^+ ions (Fig. 11) except that excitation conversion is undetectable because the excitation energies of the two Ne metastables differ by less than 0.1 eV.

Figure 15 presents photoemission spectra for Ne I radiation on Ni(100) that is clean and covered with increasing amounts of potassium. We see that increasing K adsorption reduces the intensity of the Ni d peak but produces little evidence of photoemission from the K 4s electrons. That photoemission detects the K 4s electron very weakly is more clearly seen in our data for Cu(100)-K to be presented in Sec. VI below. Earlier work on the photoemission from adsorbed alkalis shows detection to be weak[31] but to increase in intensity when the alkali layer becomes metallic at concentrations larger than that at the work-function minimum.[32]

VI. RESULTS FOR IONS INCIDENT ON CLEAN AND ALKALATED Cu(100)-K

In Fig. 16 are plotted the spectra of electrons ejected by He^+ incident on Cu(100). These data show all the features discussed for Fig. 11: the small shifts to higher energy and broadening of the clean-surface AN features in the electron distributions during the initial stages of K adsorption, the evidence in curves 3, 4, and 5 of little AD ejection by ^1S metastables, and the coincidence of the high-energy, Fermi-level side of the K 4s electron peaks in curves 5–9.

In Table II are listed the same, measured, or derived quantities for the Cu(100)-K spectra of Fig. 16 as in Table I for the Ni(100)-K spectra of Fig. 11. The values of Θ_K corresponding to our $\Delta\phi$ have been obtained from Fig. 2 for Cu(100) of Aruga *et al.*.[33] In curves 2–4 of Fig. 16 the peak or shoulder near $E-E_F=14$ eV shifts to higher energy with increasing K coverage, indicating decrease in the local work function ϕ_c' in those regions where the AN process occurs. The values of S, Θ_K, and R Cu(100) in Table II are closely similar to those for Ni(100) in Table

TABLE II. Energy shift S of the AN feature in the spectra of Cu(100)-K (Fig. 16) and the corresponding mean separation R of K atoms.

Curve	$-\Delta\phi$ (eV)	ϕ (eV)	$S=\phi_c-\phi_c'$ (eV)	Θ_K[a]	R[b] (Å)
1	0.00	4.59	0.00	0.000	∞
2	0.66	3.93	0.08	0.014	23.2
3	1.64	2.77	0.31	0.042	13.4
4	2.41	2.18	0.46	0.099	8.7
5	2.55	2.04	0.16	0.109	8.3
	2.62	1.97	0.0	0.114	8.1
6	2.65	1.94	0.0	0.12	7.9

[a]These values of Θ_K were obtained from $-\Delta\phi$ using Fig. 2 of Ref. 33.

[b]Since the edge a of the square surface unit mesh of Cu(100) is 2.56 Å we obtain $R=2.75/\sqrt{\Theta_K}$ from the relation $\Theta_K=2a^2/\sqrt{3}R^2$ for the hexagonal K unit mesh.

I. However, as is seen in the spectra of curves 5 and 6, of Fig. 16, an intermediate curve, and in the S entries of Table II, a similar peak or shoulder in this energy range shifts back to an S value of zero where it remains for the curves at still higher-K coverage not listed in Table II. We take this and the appearance of the K 4s peak in the spectra as evidence that at the coverage $\Theta_K \cong 0.10$ of curve 5 the mechanism of electron ejection is shifting from AN to RI + AD and that the peak at $S=0$ in spectra at higher-K coverage is a feature of the one-electron AD spectra in which there is no longer any AN feature. This conclusion agrees with the data of Fig. 2 of Woratschek *et al.*[14] for Cu(110), where the AN feature still visible in the spectrum at $\Theta_K=0.08$ has disappeared in the next spectrum for $\Theta_K=0.12$.

We turn now to the question as to whether the AN feature in the spectra for ions descendent from incident metastables shifts to higher energy on the $E-E_F=E_{kin}+\phi=E'_{kin}$ scale of Fig. 2 of Ref. 14 as K coverage increases. Woratschek *et al.* state that "up to $\Theta \cong 0.10\ldots$ structures arising from deexcitation at bare Cu sites ... are unshifted on the E'_{kin} scale." Certainly this is closely true on the scale of the large 2.3 eV change in the macroscopic work function. In Fig. 2 of Ref. 14 the sharp change in slope of the spectra that occurs at $E'_{kin}=10.8$ eV for $\Theta=0$ does move to higher E'_{kin} as Θ increases. But it is not easy to decide how much of this is to be attributed to the increase in intensity of the K 4s peak. There is also a possible reason why energy shifts in the AN feature could be less for the slow ions descendent from thermal metastables than for ions whose kinetic energy is 12 eV near the surface. This arises because the slower ions are more readily repelled than the faster ions from the K^+ sites and focused more on the clean sites most distant from K atoms where ϕ'_c is closest to ϕ_c. It is the low noise in our data, resulting from our use of incident ions, and the scale of 2 eV per 25.4 mm on which our data are originally plotted that enable us to measure S with sufficient accuracy.

Auger deexcitation spectra of Ni(100) and Cu(100) with our highest coverages of K are compared in Fig. 17. These spectra are remarkably similar and demonstrate that the K coverages are sufficient to mask the differing substrate electronic structures. Although the Ni d band lies just below the Fermi level and could thus be masked by the K 4s peak, the Cu d band lies between 2 and 4 eV below E_F where the AD spectrum for Cu(100)-K is of lower intensity than that for Ni(100)-K.

Photoemission spectra for He I (21.2 eV) radiation are shown in Fig. 18. Here, because the d band lies between 2 and 4 eV below E_F and the s band is of low intensity just below E_F, we can see clearly that photoemission versus Auger deexcitation has a very low probability of detection of the K 4s electrons.[31,32]

Since our only published deconvolution of an AN spectrum of clean Cu(100) was done with very early data,[27] we take this opportunity to present here the deconvolution of our present data. In Fig. 19 are plotted the AN kinetic energy distributions, $N_I(E)$ for 10 and 20 eV ions, and the derivative, $-dN_I/dE$, of the 10-eV data. Our van Cittert-type extrapolation of these data to an

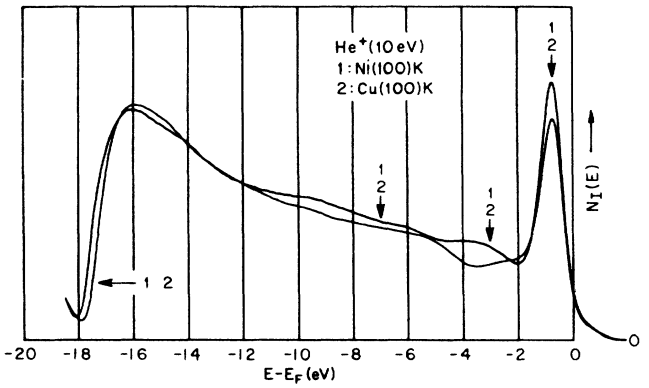

FIG. 17. Comparison of the kinetic energy distributions of electrons ejected by $He^*(^3S)$ metastables descended from the He^+ ions incident on Ni(100)-K and Cu(100)-K. Each surface has been exposed to 8×10^{-5} A's of K^+ ions.

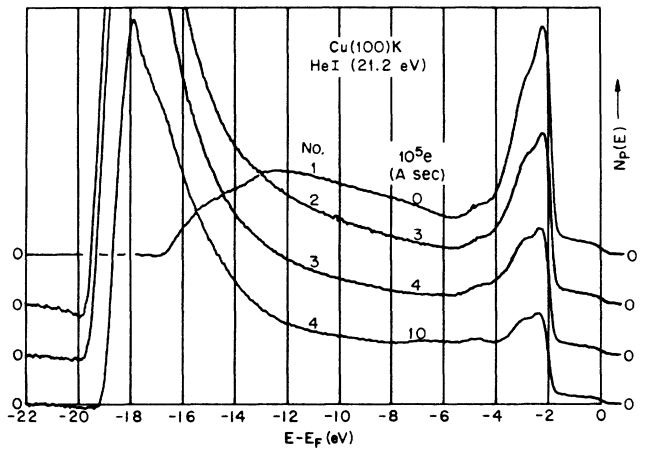

FIG. 18. He I photoemission spectra from Cu(100) with varying amounts of K adsorption. K^+ exposures are indicated at each curve.

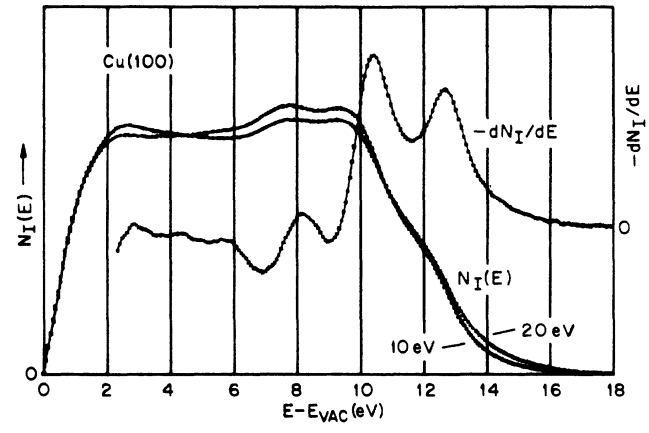

FIG. 19. Plots of the kinetic energy distributions of electrons, $N_I(E)$, ejected from clean Cu(100) by 10 and 20-eV He^+ ions. The $-dN_I/dE$ plot is the derivative of the 10-eV $N_I(E)$ distribution.

effectively zero incident kinetic energy[22] yields the fold function $F(\zeta/2)$ of Fig. 20, whose derivative $F'(\zeta/2)$ is also shown. The unfold of F by Eq. (14) of Ref. 30, gives the $U(\zeta)$ function of Fig. 20. It is the initial-state, transition-density function that is needed for comparison with the spectrum of a one-electron spectroscopy such as photoemission. This comparison is made in Fig. 21.

Our $U(\zeta)$ function of Fig. 20 for clean Cu(100) agrees in its principal features with the unfold function obtained for thermal He^+ ions on clean Cu(110) obtained with incident metastables by Sesselmann *et al.*[13] (see their Fig. 19). This agreement is dependent upon the debroadening step in our data reduction procedure since the most significant difference in the kinetic energy spectra is the greater broadening in the spectrum for the faster ions. That there is observable residual broadening in the slow ion data, however, can be seen in the tailing of the spectrum in the 13–14 eV interval of $E_{\rm kin}$ in Fig. 19 of Ref. 13. Retention of this tailing in the slow ion data is perhaps the reason why the peak nearest the Fermi level in the slow-ion deconvolution appears slightly farther from the Fermi level (greater E_B) than does the same peak in our deconvolution.

We estimate that the broadening in our data for incident ions is of the order of four times that for ions descendent from thermal metastables in the spectrum of Sesselmann *et al.* This broadening ratio, which we may call r_b, is based on the relative magnitudes of the extensions of the data beyond extrapolated maxima obtained by linear extension of the slopes at the points of inflection at highest energy. We find that we can express the atom-surface separation, $s_{\rm RI}$, at which the incident metastable undergoes RI, in terms of r_b and $s_{\rm AN}$, the separation at

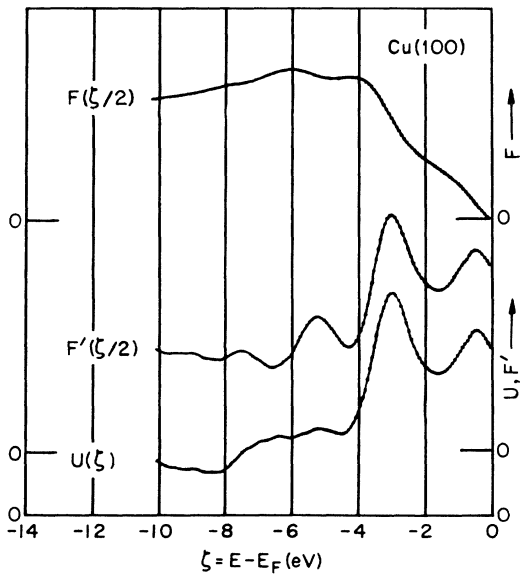

FIG. 20. The $F(\zeta/2)$ plot is the debroadened fold function obtained by a van Cittert–type extrapolation from the 10- and 20-eV $N_I(E)$ plots of Fig. 19. $F'(\zeta/2)$ is the derivative of $F(\zeta/2)$ and $U(\zeta)$ is the convolution square root of F obtained by sequential, step-midpoint deconvolution as described in Ref. 23.

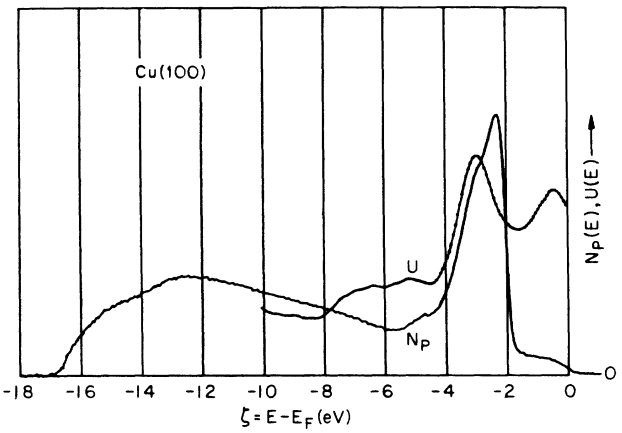

FIG. 21. Comparison of the U function of Fig. 20 with the clean-surface He I photoemission spectrum, curve 1 of Fig. 18.

which AN occurs. This makes possible a perhaps crude but nevertheless interesting exploration of the consistency among values, or limits on values, suggested for distances from a surface at which RI and AN occur.

In an earlier work on broadenings intrinsic to the AN process with incident ions it was concluded that initial-state and nonadiabatic broadenings were the two primary components, each of which varied directly with the atom's velocity.[34] The initial-state broadening results from the Heisenberg uncertainty principle and the nonadiabatic broadening from the motion of the electric charge of the ion toward the surface. The velocity dependence of these broadenings requires that, at the positions $s_{\rm AN}$ where AN occurs for ions of different velocities, r_b must equal r_v, the ratio of velocities. The ratio of kinetic energies, r_K, equals r_b^2. Since the faster ion's kinetic energy at AN is 12 eV (the 10-eV acceleration in the apparatus plus 2-eV image-force acceleration near the surface), it follows that the slow ion's kinetic energy in eV at AN should be $12/r_K = 12/r_b^2$. The increase in kinetic energy, ΔK, of the slow, descendent ion between RI and AN is thus

$$\Delta K = (12/r_K) - 0.06 \text{ eV} , \tag{6}$$

where 0.06 eV is the incident metastable's kinetic energy at RI. Since this increase in kinetic energy closely equals the change in image potential we may write

$$(3.6/s_{\rm AN}) - (3.6/s_{\rm RI}) = (12/r_b^2) - 0.06 = K[\text{eV}] . \tag{7}$$

Sesselmann *et al.*, on page 1555 of Ref. 12, have derived the value, $R = 3$ Å for the distance from the jellium edge at which AN occurs. From this and $R' = 0.6$ Å, the distance of the image plane from the jellium edge, we obtain $s_{\rm AN} = R - R' = 3 - 0.6 = 2.4$ Å. Inserting this into Eq. (7) and solving for $s_{\rm RI}$ yields an expression for the value of $s_{\rm RI}$ for ions descendent from incident thermal metastables that is consistent with our broadening ratio r_b and the $s_{\rm AN} = 2.4$ Å of Sesselmann *et al.* It is

$$s_{\rm RI} = 3.6/(1.56 - 12/r_b^2) . \tag{8}$$

This equation has the following solutions:

$$(r_b, s_{RI}) = (3.0, 15.7\ \text{Å}), (3.5, 6.2\ \text{Å}),$$
$$(4.0, 4.4\ \text{Å}), (4.5, 3.7\ \text{Å}), \text{ and } (5.0, 3.3\ \text{Å}).$$

Thus our estimate of the broadening ratio as $r_b = 4$ and the value $s_{AN} = 2.4$ Å from Sesselmann *et al.* suggests that $s_{RI} = 4.4$ Å. We do take note of the fact that s_{RI} is a rapidly varying function of r_b, particularly at smaller r_b. However, it is interesting that the result, $s_{RI} = 4.4$ Å, is the limiting atom separation suggested by Sesselmann *et al.* on page 1550 of Ref. 12 in their statement: "RI dominates over AD also in cases where R^+ is as small as about 5 Å." We recall that s_{RI} is derived from R^+ by the equation

$$s_{RI} = (R^+ - R') = 5 - 0.6\ \text{Å} = 4.4\ \text{Å}. \quad (9)$$

A larger value for s_{RI} would require a smaller broadening ratio.

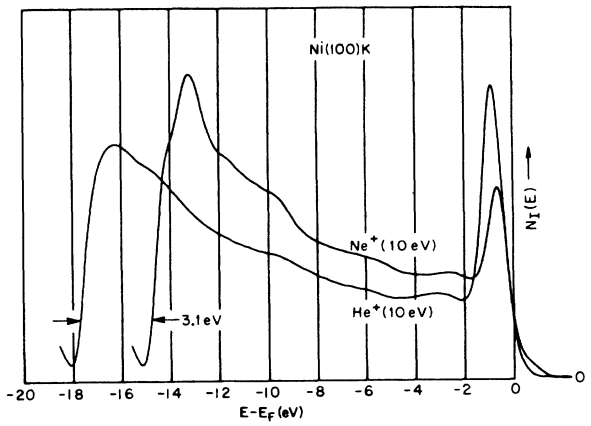

FIG. 22. Kinetic energy distributions of electrons ejected by Ne and He metastable atoms, descended from Ne^+ and He^+ ions via RN, incident on K covered Ni(100). These are curves 8 of Figs. 11 and 14. The 3.1-eV difference in spectral width demonstrates that it is the ^3S and not the ^1S He* that is the descendant of He^+.

VII. He*(^1S) TO He*(^3S) CONVERSION

The evidence for He*(^1S) to He*(^3S) conversion discussed in Sec. V was basically the magnitude of the kinetic energy of the electrons ejected by AD from the filled portion of the K (4*s*) electron resonance just below the Fermi level. Here we present another type of evidence. In Fig. 22 we compare the electron kinetic energy distributions ejected by He^+ and Ne^+ ions from the same alkalated Ni(100) surface. The evidence that almost all of the incident He^+ ions have turned into ^3S metastables before electron ejection is the 3.1 eV difference in the widths of the distributions for the two incident ions. Within experimental error 3.1 eV is equal to the difference in excitation energies between either He*($^3S_1$;19.8 eV) and Ne*($^3P_2$;16.62 eV) or He*($^3S_1$;19.8 eV) and Ne*($^3P_0$;16.72 eV). It is well outside the possible error for these differences involving He*($^1S_0$;20.62 eV). Nevertheless, a minute fraction of the electrons are ejected by ^1S metastables. This is evidenced by the difference between the two spectra of Fig. 22 to the right of E_F at $E - E_F = 0$ where the He^+ spectrum is somewhat above the Ne^+ spectrum at the energy where K (4*s*) electrons ejected by ^1S metastables should appear.

VIII. SUMMARY AND CONCLUSIONS

The present work extends the study of electron ejection from alkalated metal surfaces by ions and metastable atoms first published by Woratschek *et al.*[14] for thermal He metastables incident on Cu(100). Here we have used ions of 12-eV incident energy at the surface, both He^+ and Ne^+, and two different surfaces, Ni(100) and Cu(100). This work has corroborated that for incident metastables in many respects. Beyond this it has broadened our scope. We have shown, for example, how in the low-K-coverage regime careful measurement of spectral feature shift as more K atoms are adsorbed leads to a determination of the reduction in local work function at a so-called clean site. From this, in turn, we estimate the reduction in mean separation of the K atoms. We have also presented a deconvolution of the AN spectra for incident ions on Cu(100) and some observations based on the differences in energy broadening in the energy distributions of electrons ejected by slow and faster ions. Thus the results of studies employing incident thermal metastables and faster ions and their intercomparison have extended our understanding of the particle-solid interactions that occur when slowly moving ions and metastable atoms approach the surface of a solid.

*Present addres: 30 Sweetbriar Road, Summit, NJ 07901.

[1]H. D. Hagstrum, Phys. Rev. **96**, 336 (1954).
[2]H. S. W. Massey, Proc. Cambridge Philos. Soc. **26**, 386 (1930); **27**, 460 (1931).
[3]A. Cobas and W. E. Lamb, Jr., Phys. Rev. **65**, 327 (1944).
[4]H. D. Hagstrum, Phys. Rev. **91**, 543 (1953), Sec. V, Fig. 10; *ibid.* **96**. 336 (1954), Secs. VIII–X.
[5]L. J. Varnerin, Jr., Phys. Rev. **91**, 859 (1953).
[6]J. E. Demuth and D. E. Eastman, Phys. Rev. Lett. **32**, 1123 (1974); D. A. Shirley, Chem. Phys. Lett. **22**, 301 (1973); P. H. Citrin and D. R. Hamann, *ibid.* **22**, 301 (1973).
[7]J. R. Roussel, C. Boiziau, R. Nuvolone, and C. Reynaud, Surf. Sci. **110**, L634 (1981).
[8]H. Conrad, G. Ertl, J. Küppers, W. Sesselmann, and H. Haberland, Surf. Sci. **121**, 161 (1982)
[9]W. Sesselmann, H. Conrad, G. Ertl, J. Küppers, B. Woratschek, and H. Haberland, Phys. Rev. Lett. **50**, 446 (1983).

[10]F. Bozso, J. T. Yates, Jr., J. Arias, H. Metiu, and R. M. Martin, J. Chem. Phys. **78**, 4256 (1983).
[11]W. Sesselmann, B. Woratschek, G. Ertl, J. Küppers, and H. Haberland, Surf. Sci. **146**, 17 (1984).
[12]W. Sesselmann, B. Woratschek, J. Küppers, G. Ertl, and H. Haberland, Phys. Rev. B **35**, 1547 (1987).
[13]W. Sesselmann, B. Woratschek, J. Küppers, G. Ertl, and H. Haberland, Phys. Rev. B **35**, 8348 (1987).
[14]W. Woratschek, W. Sesselmann, J. Küppers, G. Ertl, and H. Haberland, Phys. Rev. Lett. **55**, 1231 (1985).
[15]H. D. Hagstrum, J. Vac. Sci. Technol. **20**, 626 (1982).
[16]J. Roussel, Phys. Scr. **T4**, 96 (1983).
[17]J. Lee, C. Hanrahan, J. Arias, F. Bozso, R. M. Martin, and H. Metiu, Phys. Rev. Lett. **54**, 1440 (1985).
[18]B. Woratschek, W. Sesselmann, J. Küppers, G. Ertl, and H. Haberland, Phys. Rev. Lett. **55**, 611 (1985).
[19]J. A. Appelbaum and D. R. Hamann, Phys. Rev. B **6**, 1122 (1972).
[20]N. D. Lang and W. Kohn, Phys. Rev. B **7**, 3541 (1973).
[21]The text of Sesselmann *et al.* which we are here discussing occurs on page 1555 of their paper (our Ref. 12). In it the reference to Hagstrum and Becker (their Ref. 27) is incorrect. The correct reference is to Hagstrum (their Ref. 24 and our Ref. 1) where the value discussed is given in Table VIII.
[22]H. D. Hagstrum, Phys. Rev. **150**, 495 (1966).
[23]H. D. Hagstrum, in *Electron and Ion Spectroscopy of Solids*, edited by L. Fiermans, J. Vennik, and W. Dekeyser (Plenum, New York, 1978), Sec. VIII, p. 273.
[24]R. E. Weber and L. F. Cordes, Rev. Sci. Instrum. **37**, 112 (1966).
[25]O. Heinz and R. T. Reaves, Rev. Sci. Instrum. **39**, 1229 (1968); Spectra-Mat Inc., Watsonville, CA 95076.
[26]S. Andersson and U. Jostell, Surf. Sci. **46**, 625 (1974).
[27]H. D. Hagstrum and G. E. Becker, Phys. Rev. **159**, 572 (1967).
[28]J. Lee, C. P. Hanrahan, J. Aries, R. M. Martin, and H. Metiu, Surf. Sci. **161**, L543 (1985).
[29]N. D. Lang, S. Holloway, and J. L. Nørskov, Surf. Sci. **150**, 24 (1985).
[30]R. W. Gurney, Phys. Rev. **47**, 479 (1935).
[31]S. Å. Lindgren and L. Walldén, Solid State Commun. **28**, 283 (1978).
[32]L. Waldén, Phys. Rev. Lett. **54**, 943 (1985).
[33]T. Aruga, H. Tochihara, and Y. Murata, Phys. Rev. B **34**, 8237 (1986).
[34]H. D. Hagstrum, Y. Takeishi, and D. D. Pretzer, Phys. Rev. **139**, A526 (1965).